HHS Public Access

Author manuscript

J Neurochem. Author manuscript; available in PMC 2024 January 10.

Published in final edited form as:

J Neurochem. 2023 November ; 167(4): 538–555. doi:10.1111/jnc.15979.

Gpr75 knockout mice display age-dependent cone photoreceptor cell loss

Sreelakshmi Vasudevan[1], **Ivy S. Samuels**[2,3], **Paul S.-H. Park**[1]

[1]Department of Ophthalmology and Visual Sciences, Case Western Reserve University, Cleveland, Ohio, USA

[2]Research Service, VA Northeast Ohio Healthcare System, Cleveland, Ohio, USA

[3]Department of Ophthalmic Research, Cole Eye Institute, Cleveland Clinic, Cleveland, Ohio, USA

Abstract

GPR75 is an orphan G protein-coupled receptor for which there is currently limited information and its function in physiology and disease is only recently beginning to emerge. This orphan receptor is expressed in the retina but its function in the eye is unknown. The earliest studies on GPR75 were conducted in the retina, where the receptor was first identified and cloned and mutations in the receptor were identified as a possible contributor to retinal degenerative disease. Despite these sporadic reports, the function of GPR75 in the retina and in retinal disease has yet to be explored. To assess whether GPR75 has a functional role in the retina, the retina of *Gpr75* knockout mice was characterized. Knockout mice displayed a mild progressive retinal degeneration, which was accompanied by oxidative stress. The degeneration was because of the loss of both M-cone and S-cone photoreceptor cells. Housing mice under constant dark conditions reduced oxidative stress but did not prevent cone photoreceptor cell loss, indicating that oxidative stress is not a primary cause of the observed retinal degeneration. Studies here demonstrate an important role for GPR75 in maintaining the health of cone photoreceptor cells and that *Gpr75* knockout mice can be used as a model to study cone photoreceptor cell loss.

Keywords

cone photoreceptor cell; G protein-coupled receptor; knockout mouse; orphan receptor; retina; retinal degeneration

Correspondence: Paul S.-H. Park, Department of Ophthalmology and Visual Sciences, Case Western Reserve University, Cleveland, OH 44106, USA. paul.park@case.edu.

AUTHOR CONTRIBUTIONS

Sreelakshmi Vasudevan: Data curation; formal analysis; investigation; writing – review and editing. **Ivy S. Samuels:** Investigation; methodology; writing – review and editing. **Paul S.-H. Park:** Conceptualization; formal analysis; funding acquisition; supervision; writing – original draft; writing – review and editing.

CONFLICT OF INTEREST STATEMENT

The authors report no conflicts of interest in this work.

SUPPORTING INFORMATION

Additional supporting information can be found online in the Supporting Information section at the end of this article.

1 | INTRODUCTION

GPR75 belongs to the G protein-coupled receptor (GPCR) family of membrane-spanning receptors. GPCRs are one of largest class of proteins and one of the largest class of therapeutic targets for drugs currently on the market (Sriram & Insel, 2018). A large fraction of GPCRs are orphan receptors without a known endogenous ligand and defined function (Laschet et al., 2018; Ngo et al., 2016). Thus, there is a considerably greater potential to target GPCRs in disease by determining the pharmacology and function of these orphan receptors. GPR75 was considered to be an orphan receptor, and little was known about its function (Davenport et al., 2013). GPR75 has recently been identified as the receptor for 20-hydroxyeicosatetraenoic acid (20-HETE; Garcia et al., 2017; Pascale et al., 2021). RANTES/CCL5 is also proposed to be a ligand for GPR75 (Dedoni et al., 2018; Ignatov et al., 2006; Pascale et al., 2021). Potential functional roles for GPR75 have been proposed based largely on inferences from in vitro cell culture studies. These studies have suggested possible roles for GPR75 in neuroprotection, in the function of the vasculature, diabetes, and promotion of prostate cancer metastasis (Cardenas et al., 2020; Garcia et al., 2017; Ignatov et al., 2006; Liu et al., 2013). Knockout mouse models have proven to be useful in determining the physiological or pathophysiological function of orphan GPCRs (Laschet et al., 2018; Ngo et al., 2016). Studies on *Gpr75* knockout mice have only recently begun to emerge and point to roles for GPR75 in obesity and hippocampal activity (Akbari et al., 2021; Hossain et al., 2023; Powell et al., 2022; Speidell et al., 2023).

The initial discovery and cloning of GPR75 came from examination of the Doyne's honeycomb retinal dystrophy locus in attempts to identify the causative gene for the disease (Tarttelin et al., 1999). Sequencing of DNA within this region revealed a novel GPCR, 540 amino acid residues in size. Although no causative mutations were found within the coding region for GPR75 in patients with Doyne's honeycomb retinal dystrophy, *Gpr75* transcripts were found to be localized within the retina. GPR75 was later independently identified and cloned in a study examining EST clusters derived from retinal cDNA libraries to target potential genes linked to age-related macular degeneration (AMD; Sauer et al., 2001), a retinal degenerative disorder and the leading cause of vision loss in the elderly currently without a cure (Gehrs et al., 2006). The retina expresses *Gpr75* transcripts at one of the highest levels in the human body, second only to the brain (proteinatlas.org; Sauer et al., 2001; Uhlen et al., 2015). Although GPR75 was first discovered and cloned from human retina cDNA libraries and is highly expressed in the retina, its function in the retina remains unknown and has yet to be explored in this tissue.

Dysfunction in GPR75 as a contributor to retinal disease is suggested by a genetic study of patients with AMD. Five different point mutations in *Gpr75* were identified in patients with AMD that were not detected in control patients (Sauer et al., 2001), thereby suggesting that defects in GPR75 may contribute to some pathological aspects of this age-related retinal degenerative disease. Although subsequent genetic studies have not yet confirmed a linkage between GPR75 and AMD, the possibility of GPR75 dysfunction being a contributor to retinal disease should be explored. GPR75 has been demonstrated to exhibit neuroprotective properties in cultured brain cells (Ignatov et al., 2006), and may therefore exert similar effects in neuronal cells of the retina. In the current study, a *Gpr75* knockout ($Gpr75^{-/-}$)

mouse was characterized to determine if there is a phenotype in the retina. If GPR75 plays a neuroprotective role in the retina or dysfunction in the receptor contributes to retinal disease, then the absence of the orphan GPCR should be detrimental to the health of the retina.

2 | MATERIALS AND METHODS

2.1 | Animals

All animal studies were approved by the Institutional Animal Care and Use Committee (IACUC) at Case Western Reserve University School of Medicine (Animal Welfare Assurance Number A3145–01) under protocol 2014–0021. Mice were housed in ventilated microisolator cages under a 12-h/12-h light/dark cyclic environment except for constant dark experiments, where mice were born and maintained under dim red-light conditions. Mice were provided food and water ad libitum and were housed up to 5 mice per cage until time of experiment (1–15 months of age). All experiments involving mice were terminal. Mice were killed by carbon dioxide inhalation. Animal suffering was minimized in electroretinography (ERG) experiments by anesthetizing mice and eyes and putting mice on a heating pad to maintain body temperature, as described below in the ERG section. Wild-type mice in the current study were C57Bl/6J (B6) mice (RRID:IMSR_JAX:000664). *Gpr75*$^{-/-}$ mice were generated by the trans-NIH Knock-Out Mouse Project and obtained from the KOMP Repository (www.komp.org; RRID:IMSR_KOMP:VG10647). The original mice from the KOMP repository were on a C57Bl/6N background containing the rd8 mutation (Mattapallil et al., 2012). These mice were backcrossed to B6 mice to remove the rd8 mutation. Both male and female mice were used in experiments. A total of 324 mice (B6, 149; *Gpr75*$^{-/-}$, 151; *Gpr75*$^{+/-}$, 24) were used for experiments. No exclusion criteria were pre-determined and no blinding was performed.

2.2 | RT-qPCR

Sample preparation and RT-qPCR was conducted essentially as described previously (Colozo et al., 2020; Rakshit et al., 2017). Total RNA was isolated from the retina of mice using High Pure RNA Isolation Kit (Cat# 11828665001; Roche Diagnostics) and reverse transcription was performed using the Transcriptor First Strand cDNA Synthesis Kit (Cat# 04379012001; Roche Diagnostics). qPCR was conducted in triplicate on the LightCycler 96 Real-Time PCR System (Roche Diagnostics) using the cDNA product and FastStart Essential DNA Green Master Kit (Cat# 06402712001; Roche Diagnostics). Primer sequences used are as follows: *Gpr75*, 5′-GATGC TTC CAG ACC ACA GCCAT (forward) and 5′-CCATGAGTTTGACTGTGCTGCAG, (reverse); *Gapdh*, 5′-GTGGCAAAGTGGAGATTGTTG (forward) and 5′-CGTTGAATTTGCCGTGAGTG (reverse). The threshold cycle (C_T) was determined, and the relative levels of *Gpr75* transcript were computed using the comparative C_T method using *Gapdh* as the internal control (Schmittgen & Livak, 2008). The qPCR products were also resolved by electrophoresis on a 2.5% agarose gel containing ethidium bromide (AMRESCO) and imaged on a Gel Doc XR+ System (Bio-Rad). A TriDye Ultra Low Range DNA Ladder (New England BioLabs) was also loaded on the agarose gels. Based on RT-qPCR data in (Colozo et al., 2020), a 20% difference would have 80% power with type 1 error of 5% when $n = 2$ (computed using equation 3 in Dziak et al., 2020).

2.3 | Histology and immunohistochemistry

For histology analysis, eyes were enucleated from mice and then processed, embedded in paraffin, sectioned, and stained with hematoxylin and eosin by Excalibur Pathology, as described previously (Senapati et al., 2018). Hematoxylin and eosin-stained sections were imaged on a Leica DME compound microscope equipped with an EC3 digital camera and 40×/0.65-NA objective (Leica Microsystems) or on an Axio Scan.Z1 Slide Scanner equipped with a Hitachi HV-F203 camera and a Plan Apo 20×/0.8-NA objective (Carl Zeiss Microscopy). The number of nuclei that span the outer nuclear layer (ONL) was counted manually on both superior and inferior regions at various distances from the optic nerve. For each mouse, nuclei were counted in 3 sections and then averaged. Based on histology data in (Colozo et al., 2020), a difference of 2 nuclei would have 80% power with type 1 error of 5% when $n = 3$ (computed using equation 3 in Dziak et al., 2020).

For immunohistochemistry, retinal cryosections were prepared as described previously (Colozo et al., 2020). Cone photoreceptor cell outer segments (OSs) were labeled with a 1:500 dilution of biotinylated peanut agglutinin (PNA; Vector Laboratories Cat# B-1075, RRID:AB_2313597) and then with a 1:500 dilution of streptavidin Alexa Fluor 488 conjugate (Cat# S11223; Thermo Fisher Scientific) or streptavidin Alexa Fluor 647 conjugate (Cat# S21374; Thermo Fisher Scientific). The entire cone photoreceptor cell was labeled with a rabbit anti-cone arrestin (LUMIj-mCAR) antibody (RRID:AB_2314753; Nikonov et al., 2008; Zhu et al., 2002, 2003). Rod photoreceptor cells were labeled with a mouse anti-1D4 antibody, which detects the carboxy-terminal tail of rhodopsin (Molday & MacKenzie, 1983). GPR75 was labeled with a custom rabbit polyclonal anti-GPR75 antibody generated by the Custom Polyclonal Antibody Production Service from GenScript using peptides corresponding to regions highlighted in Figure 1c. A cysteine residue was added to the sequence from GPR75 for conjugation to a carrier protein. Oxidative stress was monitored using a 1:250 dilution of rabbit anti-4-hydroxynonenal (4-HNE) antiserum (Alpha Diagnostic International Cat# HNE11-S, RRID:AB_2629282). Rabbit primary antibodies were detected with a 1:500 dilution of Alexa Fluor 488 goat anti-rabbit secondary antibody (Abcam Cat# ab150077, RRID:AB_2630356) or Alexa Fluor 568 goat anti-rabbit secondary antibody at a dilution of 1:500 (Thermo Fisher Scientific Cat# A-11011, RRID:AB_143157). Mouse primary antibody was detected with a 1:500 dilution of goat anti-mouse CF 647 secondary antibody (Cat# SAB4600183; MilliporeSigma).

Labeled retinal cryosections were generally viewed with an Olympus FV1200 confocal laser scanning microscope (Olympus) equipped with a 20×/0.75-NA objective with 2× zoom to obtain a confocal image. Images of retinal cryosections stained with anti-cone arrestin antibody were acquired with a 40×/1.40 NA oil objective, with each image representing a maximum projection of 30–36 image z-stack taken at a step size of 0.50 μm. DAPI was detected by exciting the sample with a 405 nm diode laser and the emission signal was collected at 425–460 nm. Alexa Fluor 488 was detected by exciting the sample with a multi-line ion argon laser at 473 nm and collecting the emission signal at 485–545 nm. Alexa Fluor 568 was detected by exciting the sample with a 559 nm diode laser and collecting the emission signal at 575–620 nm. Alexa Fluor 647 and CF 647 were detected by exciting the sample with a 635 nm diode laser and the emission signal was collected at

655–755 nm. For DIC imaging, TD1 detectors were used in DIC mode. To quantify staining by anti-4-HNE antibody, the threshold of images was adjusted, and the number of pixels with a signal above the threshold was quantified in ImageJ (version 1.53n).

2.4 | TUNEL assay

Apoptosis was detected using a terminal deoxynucleotidyltransferase dUTP nick-end labeling (TUNEL) assay. The TUNEL assay was applied to retinal cryosections using the DeadEnd Fluorometric TUNEL System (Promega). The sections were viewed with an Olympus FV1200 confocal laser scanning microscope (Olympus) equipped with a 20×/0.75-NA objective with 2× zoom. DAPI was detected by exciting the sample with a 405 nm diode laser and the emission signal was collected at 425–460 nm. TUNEL-positive cells were detected by exciting the sample with a multi-line ion argon laser at 473 nm and collecting the emission signal at 485–545 nm. TUNEL-positive cells in the ONL were counted using the Analyze Particles function of ImageJ (version 1.53n) by adjusting the threshold of the image.

2.5 | Electroretinography

Scotopic and photopic responses to white strobe-flash stimuli were obtained from dark-adapted mice anesthetized with 65 mg/kg pento-barbital sodium by intraperitoneal injection, as described previously (Senapati et al., 2018). Photopic responses to wavelength-specific strobe-flash stimuli were obtained as follows. Mice were dark-adapted overnight and then anesthetized with 40 mg/kg ketamine and 8 mg/kg xylazine by intraperitoneal injection. Pupils were dilated using 1% tropicamide (Bausch and Lomb), 2.5% phenylephrine hydrochloride (Akorn), and 1% cyclopentolate (Bausch and Lomb). Eyes were anesthetized with 0.5% proparacaine hydrochloride (Akorn). Mice were placed on a temperature-regulated heating pad and ERGs were recorded using an Espion E3 ColorDome full-field ganzfeld (Diagnosys). To measure cone photoreceptor cell responses, rod photoreceptor cells were first saturated with a steady-state green light-emitting diode (LED) stimulus (520 nm, half-bandwidth of 35 nm) and blue LED stimulus (445 nm, half-bandwidth of 20 nm) at an intensity of 10 cd/m^2 for 7 min. Subsequently, S-cone photoreceptor cell responses were obtained with a UV LED stimulus (365 nm, half bandwidth of 9 nm) superimposed on the steady-state background at increasing intensities of 0.0001. 0.0005, 0.002, 0.005, and 0.01 cd/m^2. M-cone photoreceptor cell responses were obtained with a green LED (520 nm, half-bandwidth of 35 nm) at increasing intensities of 2, 5, 10, 20, and 80 cd/m^2. The sampling frequency was 100 Hz with 20 responses averaged per recorded trace. The amplitude of the scotopic a-wave was measured at 6.6 ms following the stimulus. The amplitude of the scotopic b-wave was determined by summing the amplitude of the a-wave at 6.6 ms with the peak of the waveform following the oscillatory potentials. The photopic response amplitudes were calculated by summing the peak of the waveform with the amplitude at 6.6 ms. Based on ERG data in (Senapati et al., 2018), a 15% reduction in the scotopic b-wave would have 80% power with type 1 error of 5% when $n = 6$ (computed using equation 3 in Dziak et al., 2020).

2.6 | Retinal whole-mount analysis

Mouse eyes were fixed whole in 4% paraformaldehyde in PBS for 1 h prior to dissection. Retinas were dissected from the eye-cups and further fixed and flattened in 4% paraformaldehyde (in PBS) for 30 min. Retinas were washed two times in PBS (Cat# SH3025602; GE Healthcare Life Sciences) and blocked in PBST (PBS with 0.05% Tween 20, Cat# 20605; USB) containing 5% goat serum (Cat# 50062Z; Invitrogen) for 1 h with shaking. Retinas were incubated overnight at 4°C with shaking with a 1:250 dilution of rabbit polyclonal anti-S-opsin antibody (Cat# ABN1660; MilliporeSigma) or a 1:200 dilution of rabbit polyclonal anti-red/green opsin antibody (Millipore Cat# AB5405, RRID:AB_177456) in PBST containing 5% goat serum. After incubation with primary antibodies, retinal whole mounts were washed three times for 10 min in PBST and then incubated for 2 h with shaking at room temperature with Alexa Fluor 568 goat anti-rabbit secondary antibody at a dilution of 1:500 (Thermo Fisher Scientific Cat# A-11011, RRID:AB_143157). Retinas were washed two times for 10 min with PBST and then with PBS. Retinas were placed on a microscope slide with the photoreceptor cell side facing up and mounted with Prolong Diamond Antifade Mountant (Thermo Fisher Scientific). Wide-field images of fluorescently stained retinal flat mounts were acquired on a Zeiss AxioScan.Z1 equipped with a Hamamatsu ORCA-Flash4.0 v3 monochrome camera and a Plan Apo 20×/0.8-NA objective (Carl Zeiss Microscopy). Each flat mount image is comprised of multiple tiles with a z-stack of 15 μm and stitched together with the Zeiss Zen 3.1 software (Carl Zeiss Microscopy). 299 μm × 299 μm regions in both the superior and inferior retina at 600–1200 μm from the optic nerve were selected and extracted in MetaMorph 7.8 software (Molecular Devices). The number of cone photoreceptor cells, as stained by anti-M-opsin or anti-S-opsin antibodies, in those regions was quantified in ImageJ (version 1.53n) by adjusting the threshold of the image and using the Analyze Particles function. Two regions in the superior or inferior regions of the retina as shown in Figure 7 were analyzed, and the density of cone photoreceptor cells in those regions were averaged.

2.7 | Reactive oxygen species assay

Reactive oxygen species (ROS) were detected by monitoring fluorescence from dichlorofluorescein (DCF). DCF is formed when the non-fluorescent 2′,7′-dichlorofluorescin diacetate (DCFDA) reacts with ROS (Halliwell & Whiteman, 2004). Retina was dissected from mouse eyes and then homogenized in ice-cold Tris–HCl buffer (40 mM, pH 7.4). Total protein quantification was assayed using Bio-Rad Protein Assay Kit (Cat# 5000001; Bio-Rad). Retinal homogenates (100 μL) were mixed with Tris–HCl buffer (1 mL) and 10 μM DCFDA (5 μL; Sigma-Aldrich) and incubated for 30 min at 37°C. Fluorescence was measured by exciting the samples at 485 nm (5 nm slit width) and collecting the emission spectra at 525 nm (5 nm slit width) on a FluoroMax-4 spectrofluorometer (Horiba Jobin Yvon).

2.8 | Statistical analysis

Data were plotted and statistically analyzed using Prism 9 (Graph-Pad Software). Multiple comparisons were conducted using 1-way or 2-way ANOVA followed by post-hoc analysis to assess statistical significance ($p < 0.05$) of differences for individual comparisons. No

sample size calculation was performed a priori, and sample sizes used were based on previous studies (e.g., Colozo et al., 2020; Ortin-Martinez et al., 2014; Power et al., 2020; Sawant et al., 2017; Senapati et al., 2018; Trachsel-Moncho et al., 2018). The number of animals tested (*n*) is indicated in the figure legends. The data were not assessed for normality and no test for outliers was conducted. The results from statistical analyses are presented in Tables S1–S15. Qualitative experiments were conducted on at least 3 different samples to assess reproducibility.

3 | RESULTS

3.1 | Expression and localization of GPR75

The absence of GPR75 in *Gpr75*$^{-/-}$ mice was confirmed both at the transcript and protein levels. RT-qPCR demonstrated the absence of *Gpr75* transcripts in samples prepared from the retina of *Gpr75*$^{-/-}$ mice (Figure 1a,b). Immunohistochemistry was performed to confirm the absence of the GPR75 protein in the retina of *Gpr75*$^{-/-}$ mice and the localization of GPR75 in the retina of wild-type B6 mice. Commercially available antibodies for GPR75 were first tested. None of the commercially available antibodies tested, including antibodies used in previous studies (Cardenas et al., 2020, 2023; Dedoni et al., 2018; Gonzalez-Fernandez et al., 2020), demonstrated specificity for GPR75 (Figure S1). Some commercial antibodies used in previous studies were no longer available and therefore could not be tested (Garcia et al., 2017; Liu et al., 2013).

Since none of the commercial antibodies tested generated a specific signal for GPR75, we developed our own anti-GPR75 antibody. Polyclonal antibodies were generated by immunization of rabbits with three peptides that were predicted to be easily chemically synthesized and have high antigenicity. Two of the peptides corresponded to regions within the third cytoplasmic loop and a third peptide corresponded to a region within the carboxy-terminal tail (Figure 1c). Antibodies against regions within the third cytoplasmic loop did not generate a specific signal for GPR75 by immunohistochemistry (Figure 1d,e). The inability to detect GPR75 suggests that the third cytoplasmic loop may form some sort of structure that prevents access to the antibodies. Antibodies generated from a peptide within the carboxy-terminal tail, however, were able to generate a specific signal for GPR75 by immunohistochemistry (Figure 1f,g). In contrast to commercial antibodies that were tested (Figure S1), the anti-GPR75 polyclonal antibody we generated was specific for GPR75 since no labeling was detected in the retina of *Gpr75*$^{-/-}$ mice (Figure 1f). Immunohistochemistry of retina from B6 mice using our anti-GPR75 antibody indicated that GPR75 is localized in the choroid, photoreceptor, inner nuclear, and ganglion cell layers (GCLs) of the retina (Figure 1f). In the photoreceptor cell layer, the signal from GPR75 colocalized with PNA staining (Figure 1g), which labels cone photoreceptor cell OSs (Blanks & Johnson, 1984; Szel et al., 1993). Thus, GPR75 is expressed in cone photoreceptor cells.

3.2 | Retinal degeneration in *Gpr75*$^{-/-}$ mice

The health of the retina in *Gpr75*$^{-/-}$ mice was assessed by histology in animals that were 1–15 months of age. No significant difference was observed in the retina between young (1 month) B6 and *Gpr75*$^{-/-}$ mice; however, a small reduction in the number of nuclei in the

ONL was observed in older (12 months) mice (Figure 2a,b). No differences were observed in the retina of heterozygous knockout (*Gpr75*$^{+/-}$) mice at any age tested (Figure 2a,b). The number of nuclei that span the ONL, which corresponds to photoreceptor cell nuclei, was quantified to determine the progression of photoreceptor cell loss. B6 mice did not exhibit significant photoreceptor cell loss in mice aged 1–15 months (Figure 2c,f,g). *Gpr75*$^{-/-}$ mice exhibited an age-dependent mild photoreceptor cell loss (Figure 2e–g). The loss of nuclei was similar in both the inferior and superior regions of the retina. Photoreceptor cell loss was progressive with age until 12 months of age. No photoreceptor cell loss was observed in *Gpr75*$^{+/-}$ mice (Figure 2d,f,g), indicating that both alleles need to be knocked out for retinal degeneration.

Cell death was assessed by terminal deoxynucleotidyl transferase dUTP nick end labeling (TUNEL) assay (Figure 3). TUNEL-positive cells were not detected in B6 mice up until 12 months of age (Figure 3b). In contrast, TUNEL-positive cells were present in the ONL of *Gpr75*$^{-/-}$ mice, even as early as 1 month of age (Figure 3a). The peak of TUNEL-positive cells occurred at 6 months of age and tapered off thereafter (Figure 3c). This pattern of TUNEL-positive cells was consistent with the observed loss of nuclei in the outer nuclei layer, where the loss of nuclei stabilized after 12 months of age (Figure 2e–g).

3.3 | Retinal degeneration is a result of cone photoreceptor cell loss

To assess the functional consequence of the observed retinal degeneration, ERG was performed on 12-month-old B6 and *Gpr75*$^{-/-}$ mice. ERG recordings were obtained using white light under scotopic and photopic conditions. No significant differences were observed in the a-wave under scotopic conditions (Figure 4a), indicating that rod photoreceptor cells are largely unaffected by the absence of GPR75. A small difference was observed in the b-wave under scotopic conditions and a significant difference was observed in the photopic ERG response at higher light intensities (Figure 4b). In both instances, the b-wave was lower in *Gpr75*$^{-/-}$ mice compared to that in B6 mice. The lower photopic ERG responses in *Gpr75*$^{-/-}$ mice are indicative of dysfunction in cone photoreceptor cells and point to the loss of cone photoreceptor cells rather than rod photoreceptor cells in *Gpr75*$^{-/-}$ mice. Photopic ERG was also conducted on 9-month-old B6 and *Gpr75*$^{-/-}$ mice using green and UV light stimuli to examine the function of M-cone and S-cone photoreceptor cells, respectively. The photopic b-wave was lower in *Gpr75*$^{-/-}$ mice compared to B6 mice using both lighting stimuli (Figure 4c,d), indicating dysfunction of both cone photoreceptor cell subtypes.

To examine whether cone photoreceptor cell loss occurs in *Gpr75*$^{-/-}$ mice, retinal sections and whole mounts were examined. Retinal sections were labeled with an anti-1D4 antibody, which detects rhodopsin (Molday & MacKenzie, 1983), to examine the status of rod photoreceptor cells. Rhodopsin was properly localized to the OS of rod photoreceptor cells and there were no apparent differences between B6 and *Gpr75*$^{-/-}$ mice in either young (1 month) or older (12 months) mice (Figure 5). Consistent with scotopic ERG responses, rod photoreceptor cells appear to be largely unaffected in *Gpr75*$^{-/-}$ mice. Retinal sections were stained with PNA to label cone photoreceptor cell OSs and an anti-cone arrestin antibody to label the entire cone photoreceptor cell. The labeling by both PNA and anti-cone arrestin antibody in young (1 month) *Gpr75*$^{-/-}$ mice was similar to that in B6 mice (Figure

6a–d). Older (12 months) *Gpr75*$^{-/-}$ mice exhibited less PNA and anti-cone arrestin antibody staining in both the superior and inferior regions of the retina compared to age-matched B6 mice (Figure 6e–h). This reduction in PNA and anti-cone arrestin antibody staining indicates the loss of cone photoreceptor cells that is age-dependent.

To determine whether the loss of cone photoreceptor cells occurs in both cone subtypes as indicated by ERG, retinal whole mounts were labeled with anti-M-cone and anti-S-cone antibodies and the number of each cone photoreceptor cell subtype quantified (Figure 7). M cones were present throughout the retina at similar levels, whereas S cones were concentrated in the inferior region of the retina, which is the characteristic distribution of cone subtypes in B6 mice (Applebury et al., 2000; Ortin-Martinez et al., 2014). No loss of either cone subtype was detected in young (1 month) *Gpr75*$^{-/-}$ mice. In older (12 months) *Gpr75*$^{-/-}$ mice, a significant loss of M-cones was detected in both superior and inferior regions of the retina (Figure 7i). The level of S-cones was also lower in older *Gpr75*$^{-/-}$ mice in both superior and inferior regions of the retina; however, only the loss in the inferior region was deemed statistically significant (Figure 7j). Taken together, both functional and histological characterizations indicate that the retinal degeneration in *Gpr75*$^{-/-}$ mice is because of the loss of both M-cone and S-cone photoreceptor cells.

3.4 | Oxidative stress observed in the retina of *Gpr75*$^{-/-}$ mice

The retina is constantly bombarded with light and is a highly oxygenated tissue, especially in the outer retina where photoreceptor cells are present, making the retina particularly susceptible to oxidative damage (Contin et al., 2016; Youssef et al., 2011). Oxidative stress can often play a role in age-related retinal degenerations (Beatty et al., 2000; Hollyfield, 2010). Specifically, oxidative damage can cause cone photoreceptor cell death (Komeima et al., 2006; Shen et al., 2005). ROS in retinal homogenates of *Gpr75*$^{-/-}$ mice was quantified by monitoring fluorescence from DCF, which is a byproduct of the reaction between 2′,7′-dichlorofluorescein diacetate and ROS (Heidari et al., 2016). The level of ROS increased with age in both B6 and *Gpr75*$^{-/-}$ mice (Figure 8a). The amount of ROS was greater in *Gpr75*$^{-/-}$ mice compared to B6 mice. The effect of elevated ROS in the retina of *Gpr75*$^{-/-}$ mice was examined in retinal sections labeled with an anti-4-HNE antibody. 4-HNE is a byproduct of lipid peroxidation and marker for elevated ROS (Liou & Storz, 2015). The retina of *Gpr75*$^{-/-}$ mice exhibited 4-HNE staining in the photoreceptor cell layer, indicating that the elevated levels of ROS cause lipid peroxidation (Figure 8c). The levels of 4-HNE were minimal in young mice but increased with age (Figure 8b,c), mirroring the pattern of ROS quantified by DCF. The retina of B6 mice did not exhibit 4-HNE at any age tested (Figure 8d). 4-HNE staining colocalized with PNA staining (Figure 8e), indicating that elevated ROS in the retina of *Gpr75*$^{-/-}$ mice causes lipid peroxidation in cone photoreceptor cells.

Constant room lighting can cause increases in oxidative stress (Benedetto & Contin, 2019). To determine whether the lighting environment of mice contributes to the observed increase in oxidative stress and photoreceptor cell death in *Gpr75*$^{-/-}$ mice, mice were housed in constant darkness. Similar to mice housed under normal cyclic light conditions, *Gpr75*$^{-/-}$ mice housed under constant dark conditions exhibited mild retinal degeneration in older

(12 months) mice, because of the loss of cone photoreceptor cells, but not in younger (1 month) mice (Figure 9a–d). Retinal degeneration was age-dependent and occurred in both the superior and inferior regions of the retina (Figure 9e–g). Housing mice under constant dark conditions reduced the levels of ROS, as quantified by DCF fluorescence, in both B6 and *Gpr75*$^{-/-}$ mice (Figure 9h). However, retinal homogenates from *Gpr75*$^{-/-}$ mice still displayed increases in ROS that was age-dependent, and the levels were greater than that of B6 mice. Thus, light and the increases in oxidative stress that it promotes do not contribute to the cone photoreceptor cell loss observed in *Gpr75*$^{-/-}$ mice.

4 | DISCUSSION

The physiological and pathophysiological role for GPR75 is only beginning to be revealed in some tissues and diseases. The function of GPR75 in the retina is unknown despite the high expression in this tissue. Characterization of the retina of *Gpr75*$^{-/-}$ mice has revealed a potential role for the orphan receptor in cone photoreceptor cells. While systemic effects cannot be ruled out as a contributor to the observed retinal degeneration in *Gpr75*$^{-/-}$ mice, several lines of evidence support a protective role for GPR75 in cone photoreceptor cells. First, in the absence of GPR75, there is a preferential loss of cone photoreceptor cells that does not affect rod photoreceptor cell function, even up until 12 months of age (Figures 4–6). Cone loss occurs for both S-cone and M-cone photoreceptor cells (Figure 7). Second, oxidative stress accompanies photoreceptor cell loss and is detected in cone photoreceptor cells (Figure 8). Lastly, GPR75 is expressed in cone photoreceptor cells, as indicated by anti-GPR75 antibody staining (Figure 1g).

Detection of GPR75 expression in the retina was made possible by a polyclonal antibody generated against an epitope in the carboxy-terminal tail of the orphan receptor (Figure 1c). This antibody showed specificity, whereas commercial antibodies failed to exhibit specificity. Antibodies for GPCRs can lack specificity and it is essential to test in knockout animals (Michel et al., 2009). Lack of specificity of commercial anti-GPR75 antibodies was also noted previously for western blots testing material from knockout mice (Speidell et al., 2023). The expression pattern of GPR75 in the murine retina, as revealed by anti-GPR75 antibody staining (Figure 1f), shared some similarities with the predicted expression in the human retina from single-cell RNA sequencing data (proteinatlas.org; Karlsson et al., 2021). Cone photoreceptor cells are one of five cell types (others include mucus glandular cells, glandular and luminal cells, gastric mucus-secreting cells, and salivary duct cells) in the human body with enhanced expression of *Gpr75* transcripts (proteinatlas.org; Karlsson et al., 2021), thereby validating the anti-GPR75 staining in cone photoreceptor cells of the murine retina (Figure 1g). *Gpr75* transcripts are also detected in rod photoreceptor, bipolar, and Müller cells in the human retina (proteinatlas.org; Karlsson et al., 2021). Anti-GPR75 staining detected in the inner nuclear layer (INL) and GCL may correspond to expression in bipolar cells and Müller cells, which should be validated in the future. There is no evidence of anti-GPR75 staining in rod photoreceptor cells in the murine retina and rod photoreceptor cells appear to be largely unaffected in *Gpr75*$^{-/-}$ mice. Thus, there is either a disconnect between transcript and protein expression in rod photoreceptor cells or there is a difference in expression in murine and human retina.

Although oxidative stress can often play a role in age-related retinal degenerations and cause cone photoreceptor cell death (Beatty et al., 2000; Hollyfield, 2010; Komeima et al., 2006; Shen et al., 2005), it does not seem to be the primary driver of cone photoreceptor cell loss in *Gpr75*$^{-/-}$ mice. The peak of cell death occurs at 6 months of age, whereas oxidative stress keeps increasing with age even until 12 months of age (Figures 3 and 8). Furthermore, decreasing oxidative stress by housing mice under constant dark conditions does not prevent the loss of cone photoreceptor cells. (Figure 9). The progression of oxidative stress mirrors that of photoreceptor cell loss, where the loss of cone photoreceptor cells progresses with age up until 12 months of age (Figures 2f,g and 8). Thus, it appears that oxidative stress is a byproduct of cone photoreceptor cell death rather than a cause.

The nature of cone photoreceptor cell death in *Gpr75*$^{-/-}$ mice is unclear but must be investigated further to better understand the mechanism of the observed retinal degeneration. TUNEL-positive cells in *Gpr75*$^{-/-}$ mice are found throughout the ONL (Figure 3a), yet the nuclei of cone photoreceptor cells are usually present only in the apical side of the ONL (Xue et al., 2020). TUNEL-positive cells likely do not derive from rod photoreceptor cells since rods appear to be largely unaffected in *Gpr75*$^{-/-}$ mice (Figure 4a). The observed TUNEL cells may therefore represent the clearance of dying cone photoreceptor cells from the ONL (Sahaboglu et al., 2013). It is unclear why cone photoreceptor cell death does not progress further after 12 months of age. Perhaps there are protective mechanisms that become activated and prevent further loss of cone photoreceptor cells.

The specific degeneration of cone photoreceptor cells observed here in *Gpr75*$^{-/-}$ mice lends credence to a previous genetic study implicating GPR75 dysfunction in AMD (Sauer et al., 2001), where cone photoreceptor cell loss leads to blindness. Cone photoreceptor cells are essential for vision as they are required for color vision and operate under photopic conditions. In humans, cone photoreceptor cells are responsible for almost all of our vision (Lamb, 2016), and therefore preservation of vision requires the maintenance of healthy cones. Despite the importance of cone photoreceptor cells, their cell physiology and pathophysiology has been studied less than those of rod photoreceptor cells, which contribute to human vision only under restricted conditions (Lamb, 2016). This is due in part to the abundance of rod photoreceptor cells compared to cone photoreceptor cells in most mammalian retina, where cones typically make up less than 5% of the total photoreceptor cell population (Carter-Dawson & LaVail, 1979; Oyster, 1999), and the lack of appropriate mouse models. Most mouse models for retinal degenerative disease involving photoreceptor cells exhibit primary rod photoreceptor cell death (Collin et al., 2020). Cone photoreceptor cell death is secondary and studied within the context of rod photoreceptor cell death. Mouse models for primary cone photoreceptor cell death are currently scarce (Samardzija & Grimm, 2014), but required to better understand retinal degenerative diseases that primarily affect cone photoreceptor cells such as AMD. *Gpr75*$^{-/-}$ mice examined here present a novel mouse model to study a slowly progressing primary cone photoreceptor cell death in the absence of rod photoreceptor cell death.

Supplementary Material

Refer to Web version on PubMed Central for supplementary material.

ACKNOWLEDGEMENTS

We thank Heather Butler for breeding and maintaining mouse colonies, John Denker for genotyping mice, Catherine Doller for generating cryosections, and Maryanne Pendergast for help with microscopy. We thank Dr. Cheryl M. Craft (USC Roski Eye Institute and Keck School of Medicine of USC, Los Angeles, CA) for providing the anti-cone arrestin (LUMIj-mCAR) antibody. This work was funded by grants from the National Institutes of Health (R01EY021731 and P30EY011373), the Department of Veterans' Affairs (BX005844), Eversight, Retina Research Foundation, Ohio Lions Eye Research Foundation, and Cleveland Eye Bank Foundation.

All experiments were conducted in compliance with the ARRIVE guidelines.

DATA AVAILABILITY STATEMENT

Data are available on request from the authors.

Abbreviations:

4-HNE	4-hydroxynonenal
AMD	age-related macular degeneration
B6	C57Bl/6J
DCF	dichlorofluorescein
ERG	electroretinography
GCL	ganglion cell layer
GPCR	G protein-coupled receptor
INL	inner nuclear layer
IS	inner segment
ONL	outer nuclear layer
OS	outer segment
PNA	peanut agglutinin
ROS	reactive oxygen species
RRID	Research Resource Identifier
TUNEL	terminal deoxynucleotidyl transferase dUTP nick end labeling

REFERENCES

Akbari P, Gilani A, Sosina O, Kosmicki JA, Khrimian L, Fang YY, Persaud T, Garcia V, Sun D, Li A, Mbatchou J, Locke AE, Benner C, Verweij N, Lin N, Hossain S, Agostinucci K, Pascale JV, Dirice E, … Lotta LA (2021). Sequencing of 640,000 exomes identifies GPR75 variants associated with protection from obesity. Science, 373(6550), eabf8683. 10.1126/science.abf8683 [PubMed: 34210852]

Applebury ML, Antoch MP, Baxter LC, Chun LL, Falk JD, Farhangfar F, Kage K, Krzystolik MG, Lyass LA, & Robbins JT (2000). The murine cone

photoreceptor: A single cone type expresses both S and M opsins with retinal spatial patterning. Neuron, 27(3), 513–523. http://www.ncbi.nlm.nih.gov/entrez/query.fcgi?cmd=Retrieve&db=PubMed&dopt=Citation&list_uids=11055434 [PubMed: 11055434]

Beatty S, Koh H, Phil M, Henson D, & Boulton M (2000). The role of oxidative stress in the pathogenesis of age-related macular degeneration. Survey of Ophthalmology, 45(2), 115–134. 10.1016/S0039-6257(00)00140-5 [PubMed: 11033038]

Benedetto MM, & Contin MA (2019). Oxidative stress in retinal degeneration promoted by constant LED light. Frontiers in Cellular Neuroscience, 13, 139. 10.3389/fncel.2019.00139 [PubMed: 31105526]

Blanks JC, & Johnson LV (1984). Specific binding of peanut lectin to a class of retinal photoreceptor cells. A species comparison. Investigative Ophthalmology and Visual Science, 25(5), 546–557. https://www.ncbi.nlm.nih.gov/pubmed/6715128 [PubMed: 6715128]

Cardenas S, Colombero C, Cruz M, Mormandi E, Adebesin AM, Falck JR, & Nowicki S (2023). 20-HETE/GPR75 pairing modulates the expression and transcriptional activity of the androgen receptor in androgen-sensitive prostate cancer cells. Molecular and Cellular Endocrinology, 559, 111784. 10.1016/j.mce.2022.111784 [PubMed: 36202260]

Cardenas S, Colombero C, Panelo L, Dakarapu R, Falck JR, Costas MA, & Nowicki S (2020). GPR75 receptor mediates 20-HETE-signaling and metastatic features of androgen-insensitive prostate cancer cells. Biochimica et Biophysica Acta—Molecular and Cell Biology of Lipids, 1865(2), 158573. 10.1016/j.bbalip.2019.158573 [PubMed: 31760076]

Carter-Dawson LD, & LaVail MM (1979). Rods and cones in the mouse retina. I. Structural analysis using light and electron microscopy. Journal of Comparative Neurology, 188(2), 245–262. 10.1002/cne.901880204 [PubMed: 500858]

Collin GB, Gogna N, Chang B, Damkham N, Pinkney J, Hyde LF, Stone L, Naggert JK, Nishina PM, & Krebs MP (2020). Mouse models of inherited retinal degeneration with photoreceptor cell loss. Cells, 9(4), 931. 10.3390/cells9040931 [PubMed: 32290105]

Colozo AT, Vasudevan S, & Park PS (2020). Retinal degeneration in mice expressing the constitutively active G90D rhodopsin mutant. Human Molecular Genetics, 29(6), 881–891. 10.1093/hmg/ddaa008 [PubMed: 31960909]

Contin MA, Benedetto MM, Quinteros-Quintana ML, & Guido ME (2016). Light pollution: The possible consequences of excessive illumination on retina. Eye (London, England), 30(2), 255–263. 10.1038/eye.2015.221 [PubMed: 26541085]

Davenport AP, Alexander SP, Sharman JL, Pawson AJ, Benson HE, Monaghan AE, Liew WC, Mpamhanga CP, Bonner TI, Neubig RR, Pin JP, Spedding M, & Harmar AJ (2013). International Union of Basic and Clinical Pharmacology. LXXXVIII. G protein-coupled receptor list: Recommendations for new pairings with cognate ligands. Pharmacological Reviews, 65(3), 967–986. 10.1124/pr.112.007179 [PubMed: 23686350]

Dedoni S, Campbell LA, Harvey BK, Avdoshina V, & Mocchetti I (2018). The orphan G-protein-coupled receptor 75 signaling is activated by the chemokine CCL5. Journal of Neurochemistry, 146(5), 526–539. 10.1111/jnc.14463 [PubMed: 29772059]

Dziak JJ, Dierker LC, & Abar B (2020). The interpretation of statistical power after the data have been gathered. Current Psychology, 39(3), 870–877. 10.1007/s12144-018-0018-1 [PubMed: 32523323]

Garcia V, Gilani A, Shkolnik B, Pandey V, Zhang FF, Dakarapu R, Gandham SK, Reddy NR, Graves JP, Gruzdev A, Zeldin DC, Capdevila JH, Falck JR, & Schwartzman ML (2017). 20-HETE signals through G-protein-coupled receptor GPR75 (Gq) to affect vascular function and trigger hypertension. Circulation Research, 120(11), 1776–1788. 10.1161/CIRCRESAHA.116.310525 [PubMed: 28325781]

Gehrs KM, Anderson DH, Johnson LV, & Hageman GS (2006). Age-related macular degeneration—Emerging pathogenetic and therapeutic concepts. Annals of Medicine, 38(7), 450–471. 10.1080/07853890600946724 [PubMed: 17101537]

Gonzalez-Fernandez E, Staursky D, Lucas K, Nguyen BV, Li M, Liu Y, Washington C, Coolen LM, Fan F, & Roman RJ (2020). 20-HETE enzymes and receptors in the neurovascular unit: Implications in cerebrovascular disease. Frontiers in Neurology, 11, 983. 10.3389/fneur.2020.00983 [PubMed: 33013649]

Halliwell B, & Whiteman M (2004). Measuring reactive species and oxidative damage in vivo and in cell culture: How should you do it and what do the results mean? British Journal of Pharmacology, 142(2), 231–255. 10.1038/sj.bjp.0705776 [PubMed: 15155533]

Heidari R, Rasti M, Shirazi Yeganeh B, Niknahad H, Saeedi A, & Najibi A (2016). Sulfasalazine-induced renal and hepatic injury in rats and the protective role of taurine. BioImpacts: BI, 6(1), 3–8. 10.15171/bi.2016.01 [PubMed: 27340618]

Hollyfield JG (2010). Age-related macular degeneration: The molecular link between oxidative damage, tissue-specific inflammation and outer retinal disease: The Proctor lecture. Investigative Ophthalmology and Visual Science, 51(3), 1275–1281. 10.1167/iovs.09-4478

Hossain S, Gilani A, Pascale J, Villegas E, Diegisser D, Agostinucci K, Kulaprathazhe MM, Dirice E, Garcia V, & Schwartzman ML (2023). Gpr75-deficient mice are protected from high-fat diet-induced obesity. Obesity, 31(4), 1024–1037. 10.1002/oby.23692 [PubMed: 36854900]

Ignatov A, Robert J, Gregory-Evans C, & Schaller HC (2006). RANTES stimulates Ca2+ mobilization and inositol trisphosphate (IP3) formation in cells transfected with G protein-coupled receptor 75. British Journal of Pharmacology, 149(5), 490–497. 10.1038/sj.bjp.0706910 [PubMed: 17001303]

Karlsson M, Zhang C, Mear L, Zhong W, Digre A, Katona B, Sjostedt E, Butler L, Odeberg J, Dusart P, Edfors F, Oksvold P, von Feilitzen K, Zwahlen M, Arif M, Altay O, Li X, Ozcan M, Mardinoglu A, … Lindskog C (2021). A single-cell type transcriptomics map of human tissues. Science Advances, 7(31), eabh2169. 10.1126/sciadv.abh2169 [PubMed: 34321199]

Komeima K, Rogers BS, Lu L, & Campochiaro PA (2006). Antioxidants reduce cone cell death in a model of retinitis pigmentosa. Proceedings of the National Academy of Sciences of the United States of America, 103(30), 11300–11305. 10.1073/pnas.0604056103 [PubMed: 16849425]

Lamb TD (2016). Why rods and cones? Eye (London, England), 30(2), 179–185. 10.1038/eye.2015.236 [PubMed: 26563661]

Laschet C, Dupuis N, & Hanson J (2018). The G protein-coupled receptors deorphanization landscape. Biochemical Pharmacology, 153, 62–74. 10.1016/j.bcp.2018.02.016 [PubMed: 29454621]

Liou GY, & Storz P (2015). Detecting reactive oxygen species by immunohistochemistry. Methods in Molecular Biology, 1292, 97–104. 10.1007/978-1-4939-2522-3_7 [PubMed: 25804750]

Liu B, Hassan Z, Amisten S, King AJ, Bowe JE, Huang GC, Jones PM, & Persaud SJ (2013). The novel chemokine receptor, G-protein-coupled receptor 75, is expressed by islets and is coupled to stimulation of insulin secretion and improved glucose homeostasis. Diabetologia, 56(11), 2467–2476. 10.1007/s00125-013-3022-x [PubMed: 23979485]

Mattapallil MJ, Wawrousek EF, Chan CC, Zhao H, Roychoudhury J, Ferguson TA, & Caspi RR (2012). The Rd8 mutation of the Crb1 gene is present in vendor lines of C57BL/6N mice and embryonic stem cells, and confounds ocular induced mutant phenotypes. Investigative Ophthalmology and Visual Science, 53(6), 2921–2927. 10.1167/iovs.12-9662 [PubMed: 22447858]

Michel MC, Wieland T, & Tsujimoto G (2009). How reliable are G-protein-coupled receptor antibodies? Naunyn-Schmiedeberg's Archives of Pharmacology, 379(4), 385–388. 10.1007/s00210-009-0395-y [PubMed: 19172248]

Molday RS, & MacKenzie D (1983). Monoclonal antibodies to rhodopsin: Characterization, cross-reactivity, and application as structural probes. Biochemistry, 22(3), 653–660. http://www.ncbi.nlm.nih.gov/entrez/query.fcgi?cmd=Retrieve&db=PubMed&dopt=Citation&list_uids=6188482 [PubMed: 6188482]

Ngo T, Kufareva I, Coleman J, Graham RM, Abagyan R, & Smith NJ (2016). Identifying ligands at orphan GPCRs: Current status using structure-based approaches. British Journal of Pharmacology, 173(20), 2934–2951. 10.1111/bph.13452 [PubMed: 26837045]

Nikonov SS, Brown BM, Davis JA, Zuniga FI, Bragin A, Pugh EN Jr., & Craft CM (2008). Mouse cones require an arrestin for normal inactivation of phototransduction. Neuron, 59(3), 462–474. 10.1016/j.neuron.2008.06.011 [PubMed: 18701071]

Ortin-Martinez A, Nadal-Nicolas FM, Jimenez-Lopez M, Alburquerque-Bejar JJ, Nieto-Lopez L, Garcia-Ayuso D, Villegas-Perez MP, Vidal-Sanz M, & Agudo-Barriuso M (2014). Number and distribution of mouse retinal cone photoreceptors: Differences between an albino (Swiss) and a

pigmented (C57/BL6) strain. PLoS One, 9(7), e102392. 10.1371/journal.pone.0102392 [PubMed: 25029531]

Oyster CW (1999). The human eye: Structure and function. Sinauer Associates, Inc.

Pascale JV, Park EJ, Adebesin AM, Falck JR, Schwartzman ML, & Garcia V (2021). Uncovering the signalling, structure and function of the 20-HETE-GPR75 pairing: Identifying the chemokine CCL5 as a negative regulator of GPR75. British Journal of Pharmacology, 178, 3813–3828. 10.1111/bph.15525 [PubMed: 33974269]

Powell DR, Doree DD, DaCosta CM, Platt KA, Brommage R, Buhring L, Revelli JP, & Shadoan MK (2022). Mice lacking Gpr75 are Hypophagic and thin. Diabetes, Metabolic Syndrome and Obesity, 15, 45–58. 10.2147/DMSO.S342799

Power MJ, Rogerson LE, Schubert T, Berens P, Euler T, & Paquet-Durand F (2020). Systematic spatiotemporal mapping reveals divergent cell death pathways in three mouse models of hereditary retinal degeneration. Journal of Comparative Neurology, 528(7), 1113–1139. 10.1002/cne.24807 [PubMed: 31710697]

Rakshit T, Senapati S, Parmar VM, Sahu B, Maeda A, & Park PS (2017). Adaptations in rod outer segment disc membranes in response to environmental lighting conditions. Biochimica et Biophysica Acta, 1864(10), 1691–1702. 10.1016/j.bbamcr.2017.06.013 [PubMed: 28645515]

Sahaboglu A, Paquet-Durand O, Dietter J, Dengler K, Bernhard-Kurz S, Ekstrom PA, Hitzmann B, Ueffing M, & Paquet-Durand F (2013). Retinitis pigmentosa: Rapid neurodegeneration is governed by slow cell death mechanisms. Cell Death & Disease, 4(2), e488. 10.1038/cddis.2013.12 [PubMed: 23392176]

Samardzija M, & Grimm C (2014). Mouse models for cone degeneration. Advances in Experimental Medicine and Biology, 801, 567–573. 10.1007/978-1-4614-3209-8_72 [PubMed: 24664745]

Sauer CG, White K, Stohr H, Grimm T, Hutchinson A, Bernstein PS, Lewis RA, Simonelli F, Pauleikhoff D, Allikmets R, & Weber BH (2001). Evaluation of the G protein coupled receptor-75 (GPR75) in age related macular degeneration. British Journal of Ophthalmology, 85(8), 969–975. http://www.ncbi.nlm.nih.gov/entrez/query.fcgi?cmd=Retrieve&db=PubMed&dopt=Citation&list_uids=11466257 [PubMed: 11466257]

Sawant OB, Horton AM, Zucaro OF, Chan R, Bonilha VL, Samuels IS, & Rao S (2017). The circadian clock gene Bmal1 controls thyroid hormone-mediated spectral identity and cone photoreceptor function. Cell Reports, 21(3), 692–706. 10.1016/j.celrep.2017.09.069 [PubMed: 29045837]

Schmittgen TD, & Livak KJ (2008). Analyzing real-time PCR data by the comparative C_T method. Nature Protocols, 3(6), 1101–1108. https://www.ncbi.nlm.nih.gov/pubmed/18546601 [PubMed: 18546601]

Senapati S, Gragg M, Samuels IS, Parmar VM, Maeda A, & Park PS (2018). Effect of dietary docosahexaenoic acid on rhodopsin content and packing in photoreceptor cell membranes. Biochimica et Biophysica Acta, 1860(6), 1403–1413. 10.1016/j.bbamem.2018.03.030 [PubMed: 29626443]

Shen J, Yang X, Dong A, Petters RM, Peng YW, Wong F, & Campochiaro PA (2005). Oxidative damage is a potential cause of cone cell death in retinitis pigmentosa. Journal of Cellular Physiology, 203(3), 457–464. 10.1002/jcp.20346 [PubMed: 15744744]

Speidell A, Walton S, Campbell LA, Tomassoni-Ardori F, Tessarollo L, Corbo C, Taraballi F, & Mocchetti I (2023). Mice deficient for G-protein-coupled receptor 75 display altered presynaptic structural protein expression and disrupted fear conditioning recall. Journal of Neurochemistry, 165(6), 827–841. 10.1111/jnc.15818 [PubMed: 36978267]

Sriram K, & Insel PA (2018). G protein-coupled receptors as targets for approved drugs: How many targets and how many drugs? Molecular Pharmacology, 93(4), 251–258. 10.1124/mol.117.111062 [PubMed: 29298813]

Szel A, von Schantz M, Rohlich P, Farber DB, & van Veen T (1993). Difference in PNA label intensity between short-and middle-wavelength sensitive cones in the ground squirrel retina. Investigative Ophthalmology and Visual Science, 34(13), 3641–3645. https://www.ncbi.nlm.nih.gov/pubmed/8258523 [PubMed: 8258523]

Tarttelin EE, Kirschner LS, Bellingham J, Baffi J, Taymans SE, Gregory-Evans K, Csaky K, Stratakis CA, & Gregory-Evans CY (1999). Cloning and characterization of a novel orphan G-protein-

coupled receptor localized to human chromosome 2p16. Biochemical and Biophysical Research Communications, 260(1), 174–180. 10.1006/bbrc.1999.0753 [PubMed: 10381362]

Trachsel-Moncho L, Benlloch-Navarro S, Fernandez-Carbonell A, Ramirez-Lamelas DT, Olivar T, Silvestre D, Poch E, & Miranda M (2018). Oxidative stress and autophagy-related changes during retinal degeneration and development. Cell Death & Disease, 9(8), 812. 10.1038/s41419-018-0855-8 [PubMed: 30042417]

Uhlen M, Fagerberg L, Hallstrom BM, Lindskog C, Oksvold P, Mardinoglu A, Sivertsson A, Kampf C, Sjostedt E, Asplund A, Olsson I, Edlund K, Lundberg E, Navani S, Szigyarto CA, Odeberg J, Djureinovic D, Takanen JO, Hober S, … Ponten F (2015). Proteomics. Tissue-based map of the human proteome. Science, 347(6220), 1260419. 10.1126/science.1260419

Xue Y, Razafsky D, Hodzic D, & Kefalov VJ (2020). Mislocalization of cone nuclei impairs cone function in mice. FASEB Journal, 34(8), 10242–10249. 10.1096/fj.202000568R [PubMed: 32539195]

Youssef PN, Sheibani N, & Albert DM (2011). Retinal light toxicity. Eye (London, England), 25(1), 1–14. 10.1038/eye.2010.149 [PubMed: 21178995]

Zhang J, Yang J, Jang R, & Zhang Y (2015). GPCR-I-TASSER: A hybrid approach to G protein-coupled receptor structure modeling and the application to the human genome. Structure, 23(8), 1538–1549. 10.1016/j.str.2015.06.007 [PubMed: 26190572]

Zhu X, Brown B, Li A, Mears AJ, Swaroop A, & Craft CM (2003). GRK1-dependent phosphorylation of S and M opsins and their binding to cone arrestin during cone phototransduction in the mouse retina. Journal of Neuroscience, 23(14), 6152–6160. 10.1523/JNEUROSCI.23-14-06152.2003 [PubMed: 12853434]

Zhu X, Li A, Brown B, Weiss ER, Osawa S, & Craft CM (2002). Mouse cone arrestin expression pattern: Light induced translocation in cone photoreceptors. Molecular Vision, 8, 462–471. https://www.ncbi.nlm.nih.gov/pubmed/12486395 [PubMed: 12486395]

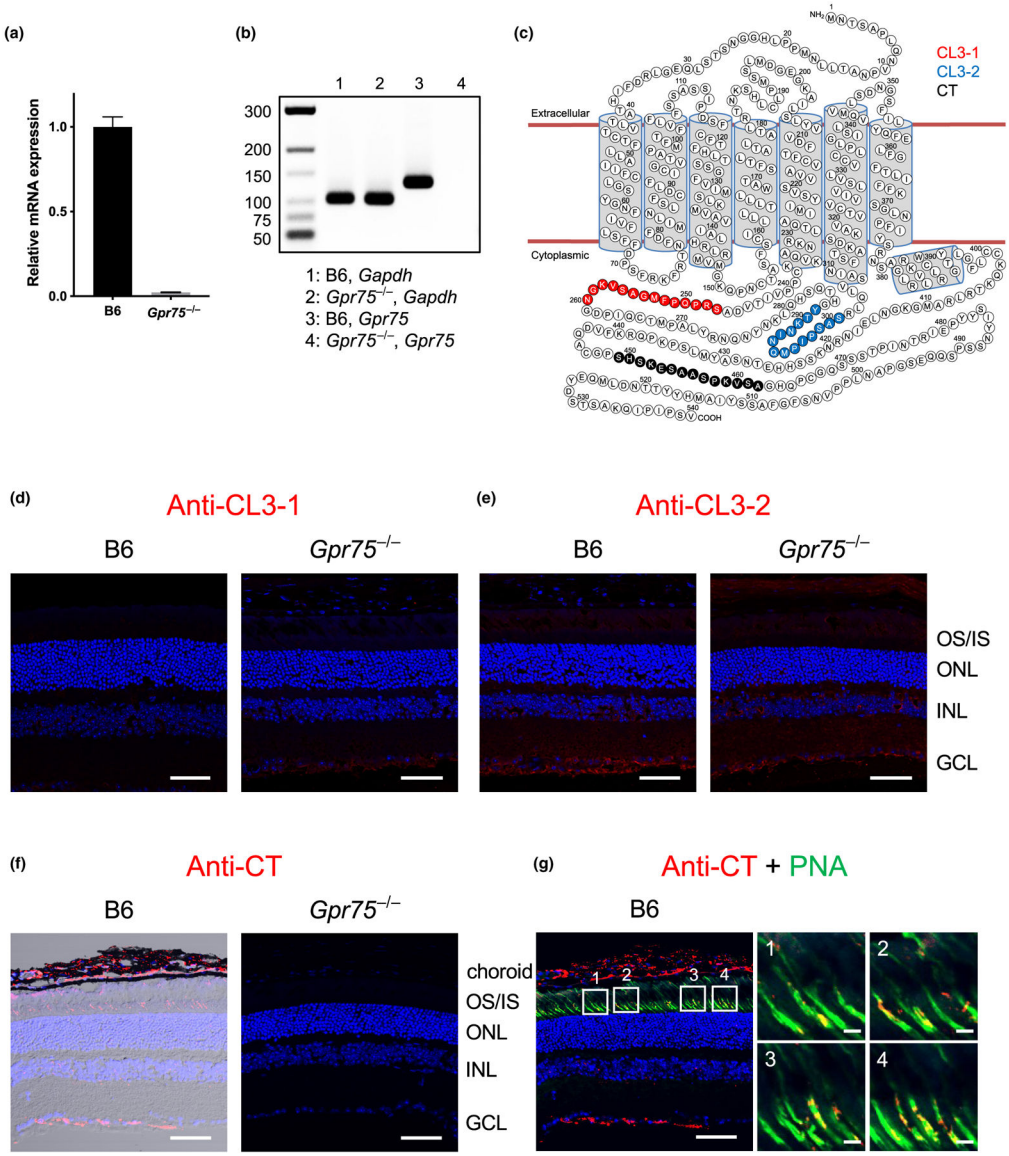

FIGURE 1.

Expression of GPR75 in the retina. (a) Quantification of *Gpr75* transcripts. The level of *Gpr75* transcripts in the retina of 3-month-old B6 and *Gpr75*$^{-/-}$ mice was quantified by RT-qPCR. The level of *Gpr75* transcripts is expressed relative to that in the retina of B6 mice. Mean values are shown with the standard deviation ($n = 3$). (b) Visualization of qPCR products. Transcripts of *Gpr75* and the internal control *Gapdh* in the retina of 3-month-old B6 and *Gpr75*$^{-/-}$ mice were resolved on a 2.5% agarose gel by electrophoresis. The corresponding number of base pairs from the DNA ladders is indicated. (c) Secondary structure of GPR75. The secondary structure of murine GPR75 was determined by GPCR-I-TASSER (Zhang et al., 2015). Peptide sequences used to generate antibodies corresponding to regions in the third cytoplasmic loop (CL3–1 and CL3–2) and cytoplasmic tail region (CT) are indicated. (d–f) Immunohistochemistry on retina from B6 and *Gpr75*$^{-/-}$ mice using anti-CL3–1 (d), anti-CL3–2 (e), and anti-CT (f) antibodies. Staining from the anti-GPR75

antibodies is indicated in red and DAPI is shown in blue. Scale bar, 50 μm. In (f) the staining of anti-CT antibody and DAPI is overlaid on the DIC image for B6 mice. (g) Colocalization of anti-CT antibody and peanut agglutinin (PNA) staining. The fluorescence microscopy image presented in (f) for B6 mice is shown with additional PNA staining (green). Areas marked by white boxes are shown as zoomed-in images on the right-hand side to more clearly observe colocalization between anti-CT antibody and PNA staining. Scale bar for zoomed-in images, 5 μm.

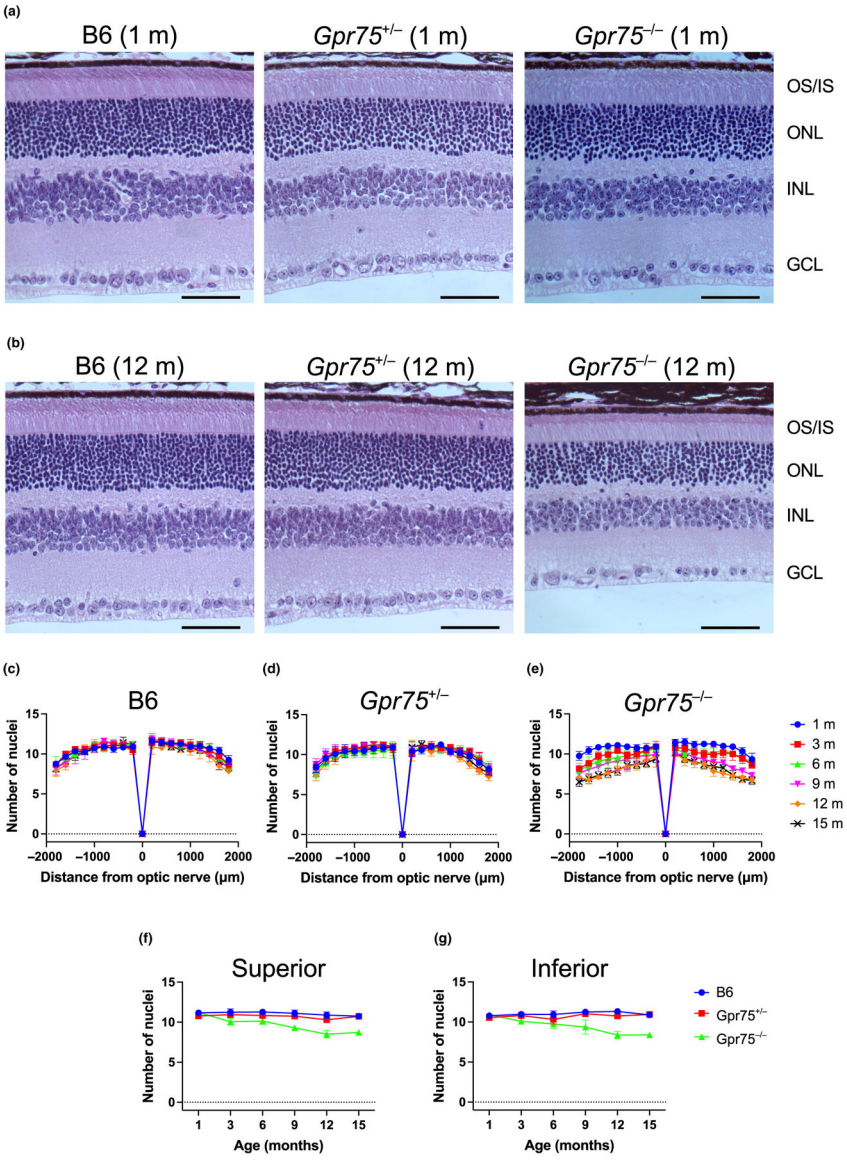

FIGURE 2.

Retinal degeneration in *Gpr75*$^{-/-}$ mice. (a, b) Hematoxylin and eosin-stained retinal sections. Retinal sections from 1-(a) and 12-(b) month-old B6, *Gpr75*$^{+/-}$, and *Gpr75*$^{-/-}$ mice are shown. Microscopy images were taken from the superior region about 600–1000 μm from the optic nerve. The outer segment (OS)/inner segment (IS) of photoreceptor cells, outer nuclear layer (ONL), inner nuclear layer (INL), and ganglion cell layer (GCL) are indicated. Scale bar, 50 μm. (c–e) Quantification of the number of nuclei that span the ONL. The number of nuclei was quantified at different distances from the optic nerve in the superior (positive) or inferior (negative) regions of the retina of B6, *Gpr75*$^{+/-}$, and *Gpr75*$^{-/-}$ mice at ages 1–15 months. Mean values are shown with the standard deviation ($n = 4$). (f, g) Progressive retinal degeneration. The number of nuclei that span the ONL at distances of 600, 800, and 1000 μm from the optic nerve in the superior (f) and inferior (g) regions of

the retina was averaged and plotted versus the age of mice. Mean values are shown with the standard deviation ($n = 4$). Statistical analyses are presented in Tables S1 and S2.

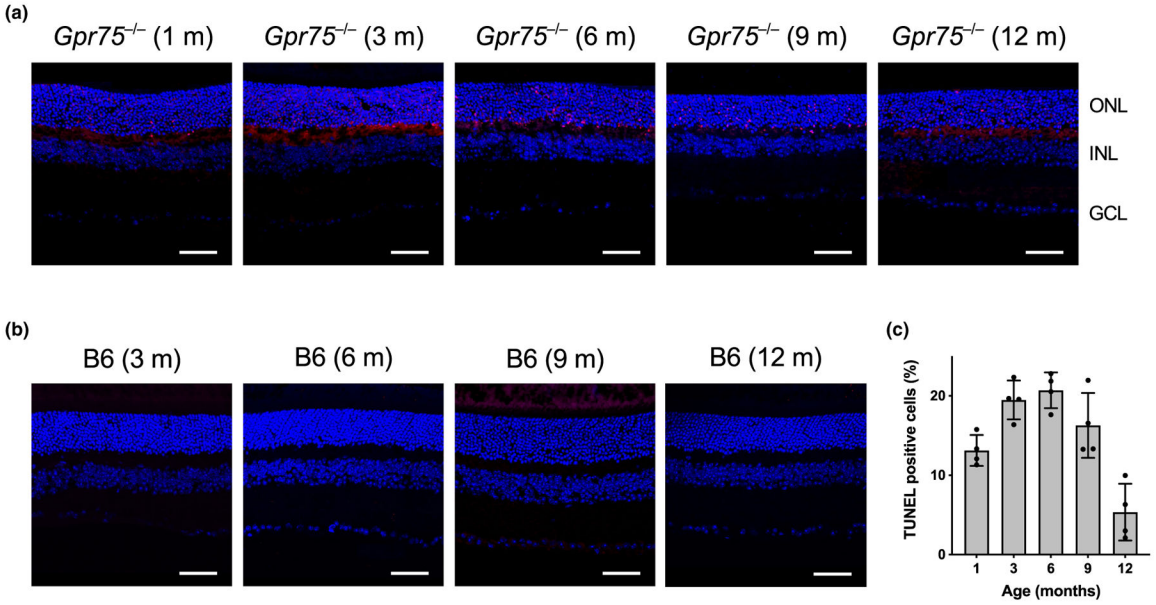

FIGURE 3.

TUNEL assay on the retina of B6 and *Gpr75*$^{-/-}$ mice. (a, b) TUNEL assay on the retina of different aged mice. TUNEL staining (red) is observed in the outer nuclear layer (ONL) of *Gpr75*$^{-/-}$ mice (a) but not B6 mice (b). DAPI staining is shown in blue. ONL, inner nuclear layer (INL), and ganglion cell layer (GCL) are indicated. Scale bar, 50 μm. (c) Quantification of TUNEL-positive cells in *Gpr75*$^{-/-}$ mice. The number of TUNEL-positive cells in the ONL was quantified in mice 1–12 months of age. Mean values are shown with the standard deviation ($n = 4$). Statistical analyses are presented in Table S3.

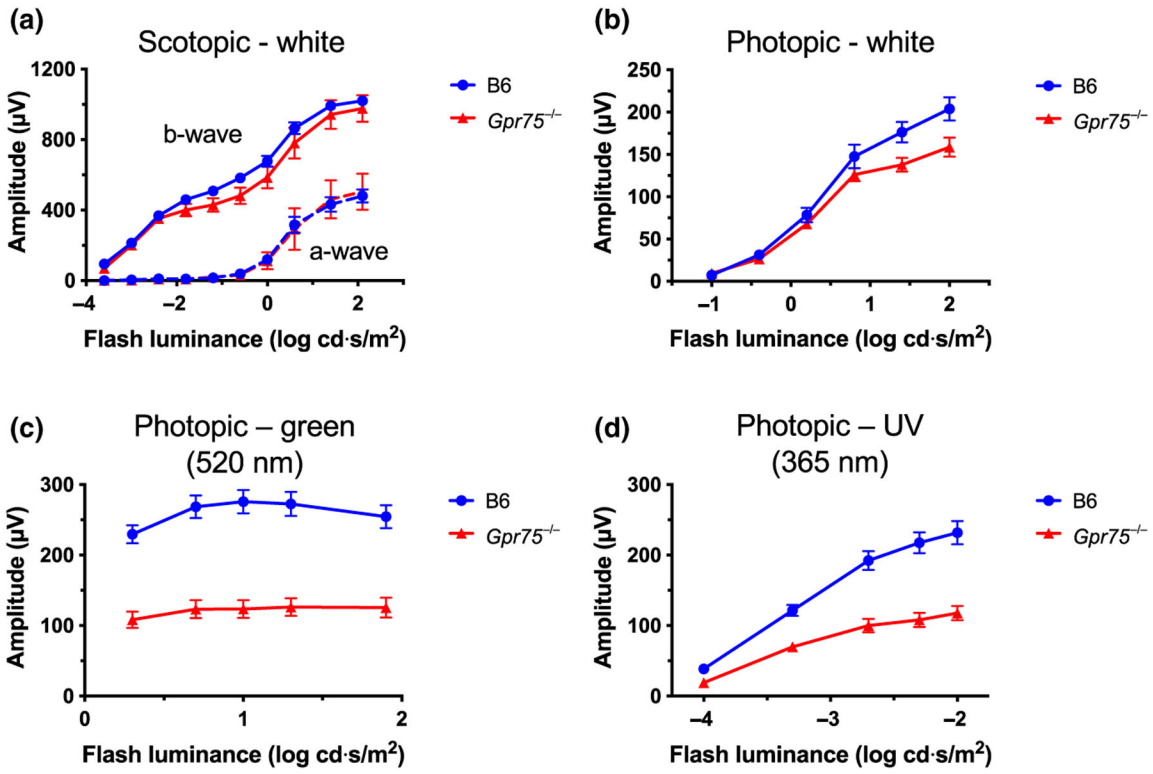

FIGURE 4.

Cone photoreceptor cell dysfunction. (a, b) Electroretinography (ERG) recordings were obtained from 12-month-old B6 ($n = 4$) and *Gpr75*$^{-/-}$ mice ($n = 6$) mice at increasing intensities of white light flashes under scotopic (a) or photopic (b) conditions. Both a-waves (dashed line) and b-waves (solid line) are plotted for scotopic conditions, and only b-waves are plotted for photopic conditions. (c, d) Photopic ERG recordings were obtained from 9-month-old B6 ($n = 7$) and *Gpr75*$^{-/-}$ ($n = 7$) mice at increasing intensities of green (c) or UV (d) light flashes and the b-wave responses are plotted. Mean values are plotted along with the standard error of the mean. Sample ERG waveform traces for each condition are presented in Figure S2, and statistical analyses of the data are presented in Tables S4–S8.

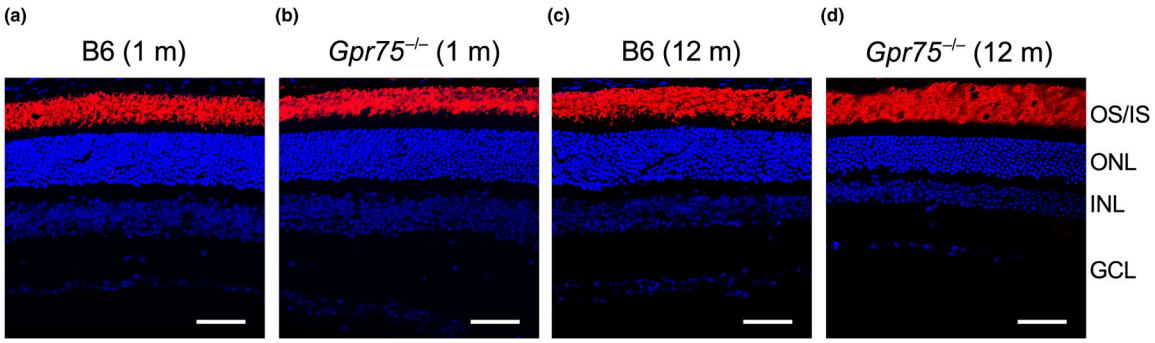

FIGURE 5.

Rod photoreceptor cells unaffected in *Gpr75*$^{-/-}$ mice. Cryosections were prepared from the retina of 1-month-old B6 (a) and *Gpr75*$^{-/-}$ (b) mice and 12-month-old B6 (c) and *Gpr75*$^{-/-}$ (d) mice. Rod photoreceptor cells were labeled with an anti-1D4 antibody (red), which detects rhodopsin, and nuclei were labeled with DAPI (blue). Microscopy images from a region within 600–1000 μm from the optic nerve in the superior retina are shown. The outer segment (OS)/inner segment (IS) of photoreceptor cells, outer nuclear layer (ONL), inner nuclear layer (INL), and ganglion cell layer (GCL) are indicated. Scale bar, 50 μm.

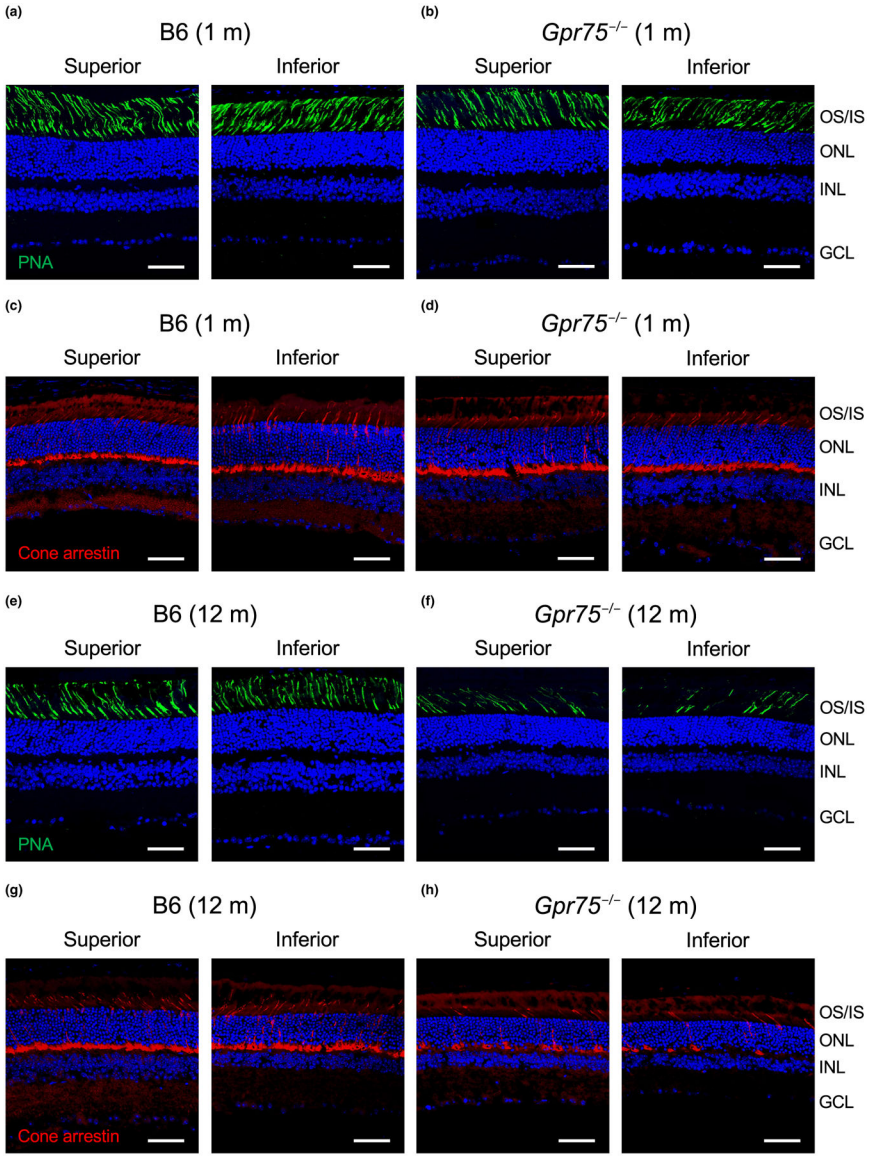

FIGURE 6.

Loss of cone photoreceptor cells in *Gpr75*$^{-/-}$ mice. Cryosections were prepared from the retina of 1-month-old B6 (a, c) and *Gpr75*$^{-/-}$ (b, d) mice and 12-month-old B6 (e, g) and *Gpr75*$^{-/-}$ (f, h) mice. Cone photoreceptor cell outer segments were labeled with peanut agglutinin (PNA; green), entire cone photoreceptor cells were labeled with an anti-cone arrestin antibody (red), and nuclei were labeled with DAPI (blue). Microscopy images from a region within 600–1000 μm from the optic nerve in either the superior or inferior retina are shown. The outer segment (OS)/inner segment (IS) of photoreceptor cells, outer nuclear layer (ONL), inner nuclear layer (INL), and ganglion cell layer (GCL) are indicated. Scale bar, 50 μm.

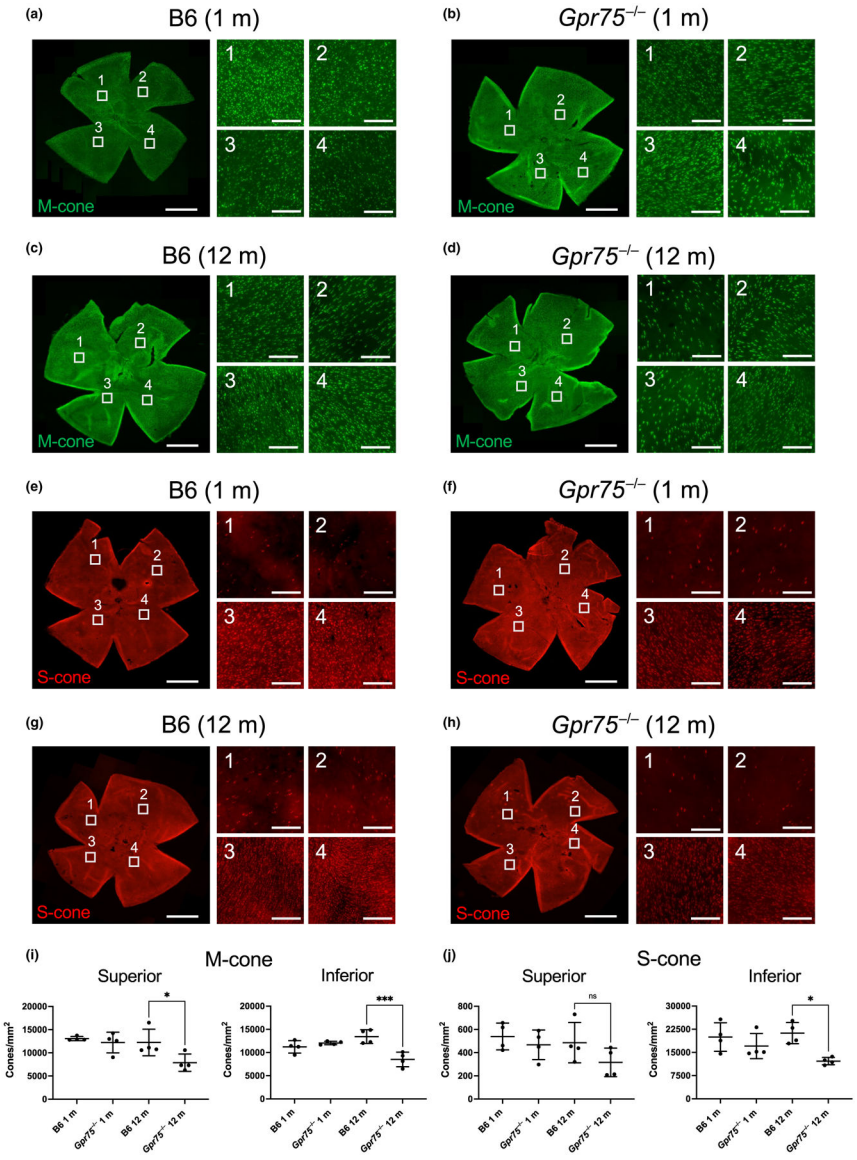

FIGURE 7.

Cone photoreceptor cell loss occurs in both M-cone and S-cone photoreceptor cells. (a–h) Retinal whole mounts prepared from 1-month or 12-month-old B6 and *Gpr75*$^{-/-}$ mice were stained with either anti-M-cone (green) or anti-S-cone (red) antibodies. The superior retina is at the top, and inferior retina is at the bottom. Regions indicated by white boxes on whole-mount images are shown as zoomed-in images on the right-hand side. Whole-mount scale bar, 1 mm. Zoomed-in image scale bar, 100 μm. (i, j) Quantification of M-cone (I) and S-cone (J) photoreceptor cells in whole mounts. The density of M-cone or S-cone photoreceptor cells in the superior (left graph) or inferior (right graph) regions of the retina are plotted. Mean values with the standard deviation are shown ($n = 4$). Asterisks indicate significant differences ($p < 0.05$). Statistical analyses of the data are presented in Table S9.

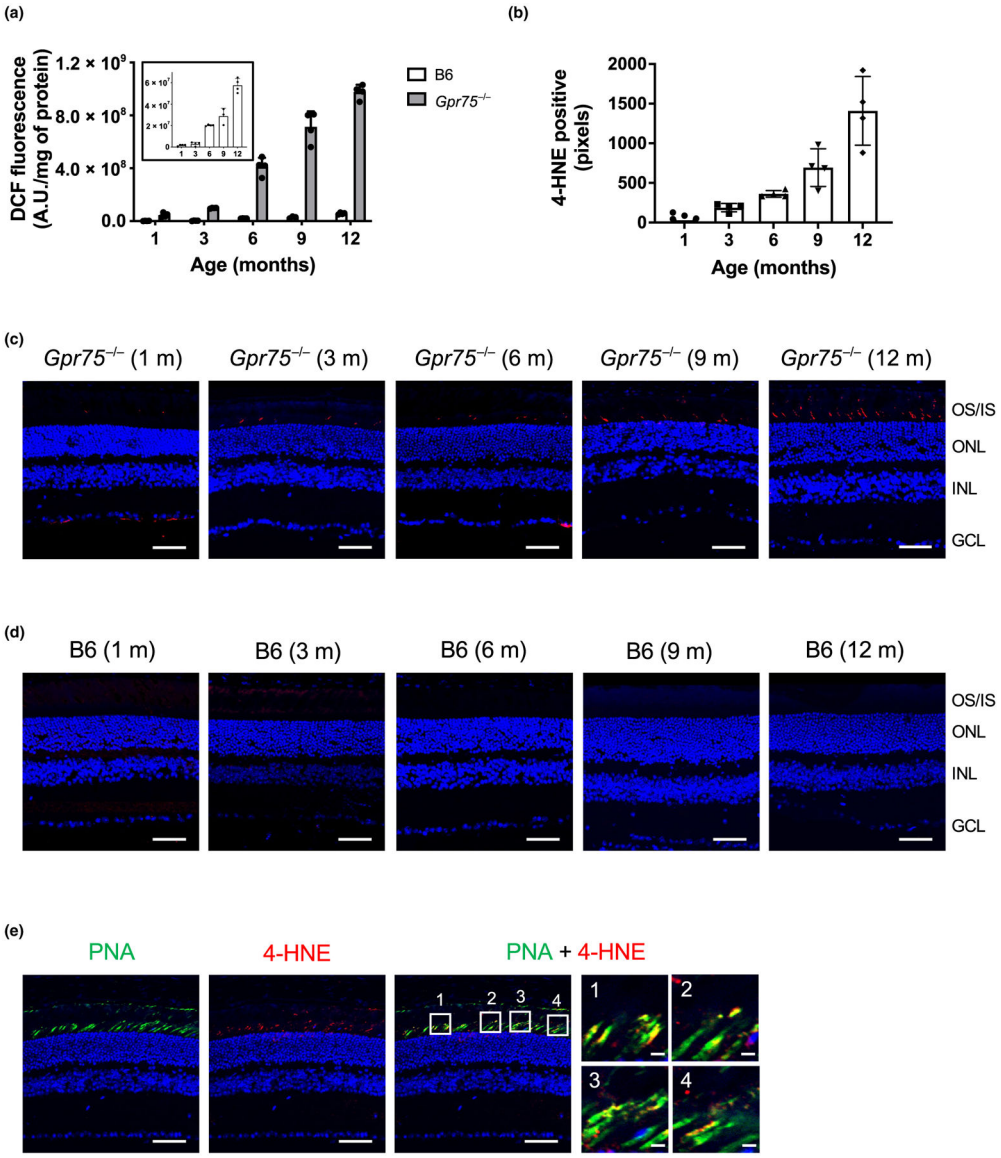

FIGURE 8.

Increased oxidative stress accompanies retinal degeneration in *Gpr75*$^{-/-}$ mice. (a) Reactive oxygen species (ROS) in retinal homogenates. ROS was quantified by monitoring fluorescence from dichlorofluorescein (DCF) in retinal homogenates from B6 and *Gpr75*$^{-/-}$ mice of different ages. Mean values with associated standard deviations are shown ($n = 4$). (b) Quantification of 4-HNE staining in retinal cryosections. The number of pixels exhibiting 4-HNE staining from immunohistochemistry was quantified from retinal cryosections of *Gpr75*$^{-/-}$ mice of different ages (e.g., (c)). Mean values with associated standard deviations are shown ($n = 4$). Statistical analyses of the data are presented in Tables S10–S12. (c, d) 4-HNE staining in retinal cryosections from *Gpr75*$^{-/-}$ (c) and B6 (d) mice that were 1–12 months of age. 4-HNE was detected with an anti-4HNE antibody (red). DAPI staining is shown in blue. The outer segment (OS)/inner segment (IS) of photoreceptor cells, outer nuclear layer (ONL), inner nuclear layer (INL), and ganglion cell layer (GCL)

are indicated. Scale bar, 50 μm. (e) Retinal cryosection from 12-month-old *Gpr75*$^{-/-}$ mouse stained with peanut agglutinin (PNA; green) or anti-4HNE antibody (red). Scale bar, 50 μm. A merged image is shown along with zoomed-in images (scale bar, 5 μm) from regions indicated by white boxes.

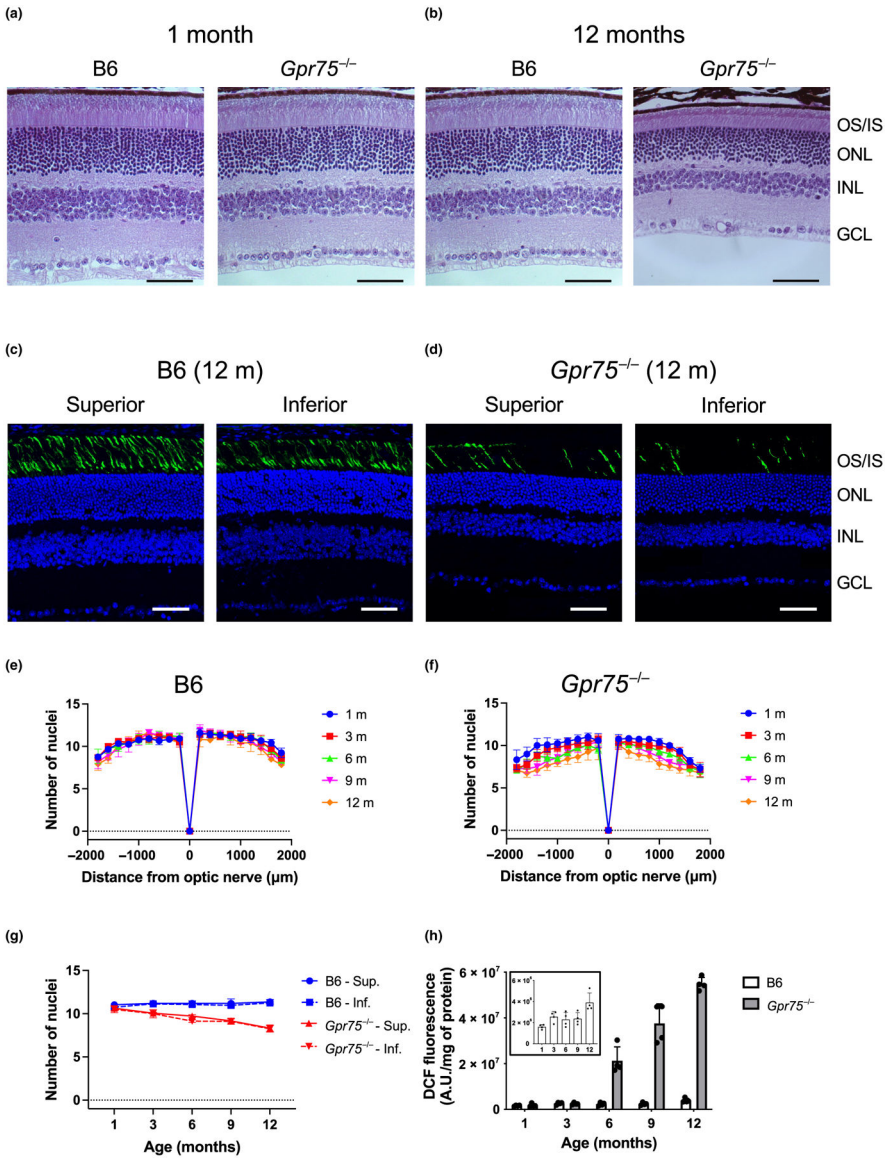

FIGURE 9.

Mice housed under constant dark conditions still exhibit retinal degeneration in *Gpr75*$^{-/-}$ mice. (a, b) Hematoxylin and eosin-stained retinal sections from mice housed under constant dark conditions. Retinal sections from 1-(a) and 12-(b) month-old B6 and *Gpr75*$^{-/-}$ mice are shown. Microscopy images were taken from the superior region about 600–1000 μm from the optic nerve. (c, d) Cryosections were prepared from the retina of 12-month-old B6 (c) and *Gpr75*$^{-/-}$ (d) mice. Cone photoreceptor cells were labeled with peanut agglutinin (PNA; green) and nuclei were labeled with DAPI (blue). Microscopy images from a region within 600–1000 μm from the optic nerve in either the superior or inferior retina are shown. The outer segment (OS)/inner segment (IS) of photoreceptor cells, outer nuclear layer (ONL), inner nuclear layer (INL), and ganglion cell layer (GCL) are indicated. Scale bar, 50 μm. (e, f) Quantification of the number of nuclei that span the ONL in the superior (positive) or inferior (negative) region of the retina of B6 (e) and *Gpr75*$^{-/-}$ mice (f). (g) The number

of nuclei that span the ONL at distances of 600, 800, and 1000 μm from the optic nerve in the superior and inferior regions of the retina was averaged and plotted versus the age of mice. Mean values are shown with the standard deviation ($n = 4$). (h) Reactive oxygen species (ROS) in retinal homogenates of B6 and *Gpr75*$^{-/-}$ mice housed under constant dark conditions. ROS was quantified by monitoring dichlorofluorescein (DCF) fluorescence in retinal homogenates. Mean values are presented with the standard deviation ($n = 4$). The inset shows values for B6 mice on a magnified scale. Statistical analyses of the data are presented in Tables S13–S15.